Turkish Journal of Electrical Engineering & Computer Sciences

http://journals.tubitak.gov.tr/elektrik/

Research Article

Turk J Elec Eng & Comp Sci
(2021) 29: 1241 – 1258

doi:10.3906/elk-1908-62

Sliding mode PLL-PDM controller for induction heating system

Harun ÖZBAY[1,*], **Akif KARAFİL**[2], **Selim ÖNCÜ**[3]

[1]Department of Electrical Engineering, Faculty of Engineering and Natural Sciences, Bandırma Onyedi Eylül University, Balıkesir, Turkey

[2]Department of Electrical and Electronics Engineering, Faculty of Engineering, Yalova University, Yalova, Turkey

[3]Department of Electrical and Electronics Engineering, Faculty of Engineering, Karabük University, Karabük, Turkey

Received: 11.08.2019 • **Accepted/Published Online:** 16.11.2020 • **Final Version:** 30.03.2021

Abstract: In this study, a sliding mode controlled phase locked loop (SMC-PLL) was developed for induction heating (IH) applications with a resonant inverter. PLL applications are widely used in induction heating applications to achieve zero voltage switching and zero current switching. In many PLL applications, the frequency tracking is too slow and unreliable. Therefore, a sliding mode controller was developed to provide robust and fast PLL. Furthermore, a pulse density modulation (PDM) control strategy was developed to work at the resonant frequency for all power levels. The PDM power control is a good solution for the design of high-frequency inverters because of a great reduction of switching losses and electromagnetic noise. The PDM pattern for the desired output power is determined according to the set temperature value of the work piece. The proposed system was simulated in PSIM and a 250-W laboratory prototype was implemented with operating frequency of 35–42 kHz.

Key words: Sliding mode control, pulse density modulation, phase locked loop, series resonant inverter, induction heating

1. Introduction

Induction heating (IH) is used in many industrial and domestic applications such as surface hardening, melting, annealing, and cooking [1, 2] since it has many advantages over conventional heating systems (resistance, ignition, etc.). These advantages include short processing time, uniform heat dissipation, high efficiency, and avoiding hazards such as combustion and explosion. In addition, no waste is generated at the end of an IH process [3]. All of these advantages indicate that induction heating is a reliable method for heating. In IH systems, the AC current used to generate an electromagnetic field is achieved by the use of many different DC-AC converter structures [4]. Factors such as input voltage, ease of control, efficiency, power, cost, and operating frequency are taken into account when determining the inverter structure. On the other hand, a half bridge and a full bridge are generally preferred in medium- and high-power applications, respectively [5]. Soft switching techniques such as zero voltage switching (ZVS) and zero current switching (ZCS) are generally used to reduce switching losses in these converters. ZCS is suitable for insulated-gate bipolar transistor due to the tail current at low switching frequencies, but not suitable for metal–oxide–semiconductor field-effect transistors (MOSFETs) preferred at high switching frequencies. This is because MOSFET's turn-on losses are more dominant than turn-off losses. Therefore, especially when MOSFETs are used as switches for high switching frequencies, ZVS is

*Correspondence: hozbay@bandirma.edu.tr

preferred to reduce turn-off losses [6–8]. However, MOSFET's turn-off losses cannot be prevented. Furthermore, if the quality factor of the resonant circuit is not high enough, the turn-off losses will increase and therefore can have devastating effects on the switches. As a result, the efficiency of the inverter is reduced and the power switches may be damaged. In this condition, the inverter is operated at a resonant frequency where switching losses are completely eliminated to avoid these adverse conditions. At the resonant frequency, the switches are continuously switched on and off under conditions of ZCS so that switching losses are avoided. However, in such applications, the resonant frequency connected to the resonant elements must be continuously tracked since the values of these elements may change over time due to the environmental and physical factors. Therefore, the PLL algorithm is generally preferred in tracking the resonant frequency [9, 10]. PLL schemes are generally used to synchronize the inverter and the switching frequency [11–14]. In this process, the phase shift between the current and the voltage is passed through an XOR gate and the output is measured by filtering through the low-pass filter. Then a voltage-controlled oscillator (VCO) generates signals for the switches. Integrated circuits (ICs) such as 4046-family are generally used in the implementation of this control scheme [15–18]. Although the analog control with ICs has been proven to be effective, accurate, and widely used in IH applications today, it is less flexible and less resistant to variations than the digital control. Therefore, the SMC algorithm, which has a robust control, simple application, and fast response even under all system parameters, was used to track the resonant frequency and to provide effective control in nonlinear systems [19, 20]. One of the most important challenges encountered when designing an IH system is power control. Many control methods (PWM, frequency, phase shift, etc.) are used in the power control of the inverters. When these control methods are examined, it is seen that there are various advantages and disadvantages compared to each other. In the PWM control method, the power control is provided by changing the duty ratio of the switches in the inverter. However, the efficiency of the system is low since the resonant cannot be achieved at every power level [21]. In the frequency control method, the power control is achieved by changing the switching frequency. However, as the operating frequency of the inverter moves away from the resonant frequency, the circuit current decreases. In this case, the sine waveform of the current is also disrupted. In the phase shift control method, power control is performed by controlling the switching states of both bridge legs and by adjusting the phase shift between them. However, in this method, soft switching is also not achieved at every power level [22]. In these control methods, switching losses and electromagnetic interference (EMI) are quite high and soft switching cannot be performed at all power levels. Pulse density modulation (PDM) is one of the alternative solutions for these problems [23–25]. In this study, a PDM control technique based on the principle of deleting some of the switching signals was used in order to enable the system to control the power by providing the soft switching conditions at each power level. This paper is organized as follows: Section 2 presents the system design and analysis. This section includes the design of a series resonant converter for induction heating, the analyzed PDM control strategy and a sliding mode controlled PLL. In Section 3, the PSIM simulation of the proposed system is presented. Section 4 gives information about the experimental study and analyses results. Finally, some conclusions are drawn in the conclusion section.

2. Design and analysis of a sliding mode controlled induction heater

The proposed IH system in Figure 1 consists of series resonant inverter, control, and measurement layers. The DC source at the input is converted to a high-frequency AC voltage using a series resonant inverter. Therefore, high-frequency current is provided to the induction coil. In order to monitor the resonant frequency of the inverter, a sliding-mode controlled phase locking loop (SMC-PLL) is used. PDM signals are generated and

applied to the switches in order to keep the work piece of the resonant frequency constant at the desired temperature.

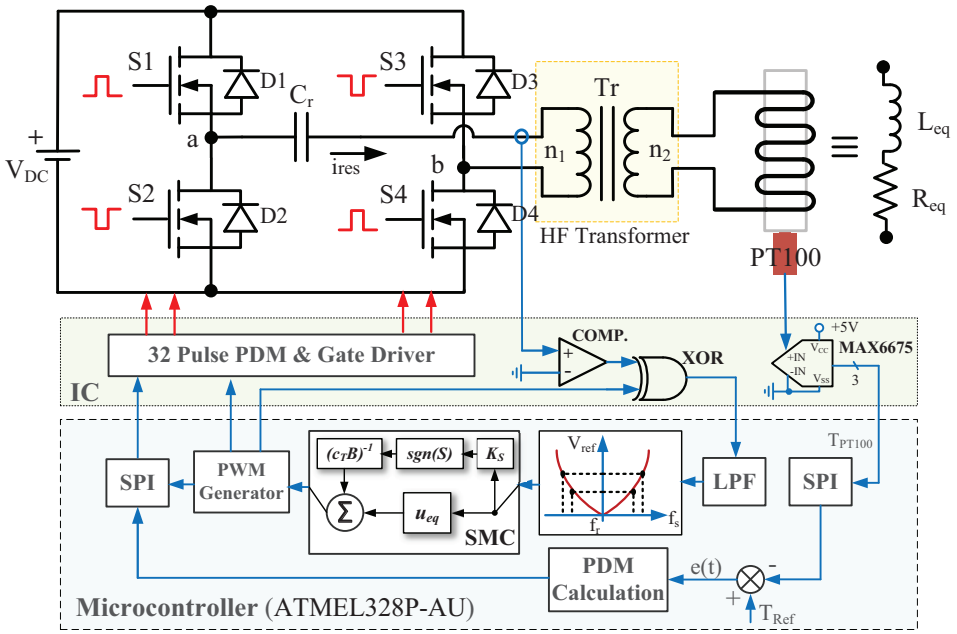

Figure 1. The configuration of the proposed system.

2.1. Series resonant inverter for induction heater

Induction heating is the process of heating a work piece with losses occurring on the material by forming eddy currents in the metal work piece that is placed in a time-varying electromagnetic field [4]. During this process, eddy and hysteresis losses occur on the material which are not desired under normal conditions in an electrical machine. These losses cause the work piece to warm up. Induction heating systems have many advantages over conventional heating methods. In conventional methods, while external heating is required to heat the material, in induction heating systems heating is performed by utilizing the structure of the material itself. In this way, the heat is not emitted to the environment and the heating process is more efficient and faster. Therefore, it works with higher efficiency. Since these systems are microcontroller-controlled, sensitive power control can be achieved [1]. One of the circuit topologies commonly used in induction heating systems is the full-bridge series resonant inverter shown in Figure 1. The full-bridge series resonant inverter consists of a DC voltage source and four power switches. When the switches S1 and S4 are switched on, the input voltage is obtained at the load ends. On the other hand, when the switches S2 and S3 are switched on, the input voltage of the $-V_{DC}$ at the load ends is obtained. The equivalent circuit and operating modes of the system are shown in Figure 2.

In Mode I, S1 and S4 switches, and in Mode II, S2 and S3 switches are on. In Mode III, the inverter output voltage (Vab) is zero. In this mode, when S2 is on, the current passing on through D4 is in the form of damped oscillation, and when S4 is on, the current passing on through D2 is in the form of damped oscillation. Since the series resonant circuit will be used in the induction heating application, it must be in low damping condition by providing the Equation 1 condition [10].

$$\omega_r > a \tag{1}$$

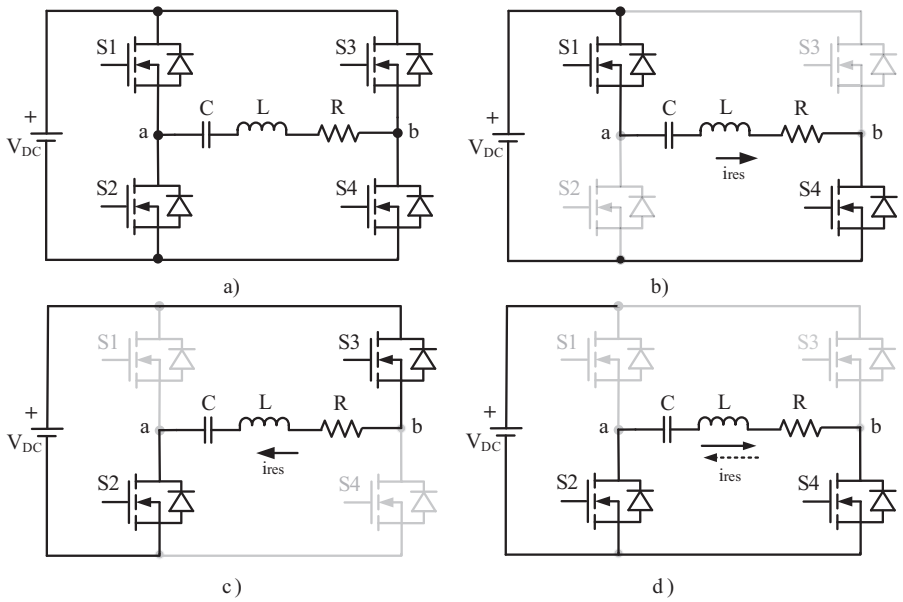

Figure 2. Simplified circuit operating modes: (a) equivalent the circuit, (b) Mode I, (c) Mode II, and (d) Mode III.

In this equation, ω_r represents the resonant angular frequency and a represents the damping coefficient. The equations of resonant angular frequency and the damping coefficient are given in Equations 2 and 3, respectively.

$$\omega_r = \frac{1}{\sqrt{LC}} \tag{2}$$

$$a = \frac{R}{2L} \tag{3}$$

The resonant frequency of the circuit is presented by Equation 4.

$$f_r = \frac{1}{2\pi\sqrt{LC}} \tag{4}$$

The reflected resistance in the equivalent circuit is calculated by Equation 5.

$$R = (\frac{n_1}{n_2})^2 R_{eq} \tag{5}$$

In this equation, R_{eq} is the effective resistance and n_1/n_2 is the transformer ratio. The frequency response of the filter in the inverter can be expressed in terms of the quality factor calculated in Equation 6.

$$Q = \frac{\omega_r L}{R} \tag{6}$$

2.2. Analysis of PDM control strategy

The PDM control technique is a set of commands. Power control is performed by deleting some of the control pulses according to the command sequences without any changes in the switching frequency and the transmission time of the switch. The output power of the converter decreases as the number of the deleted control pulses increases [23]. Figure 3a shows the PDM switching patterns for N = 32. As shown in Figure 3b, in the three resonant cycles, the square wave voltage (in the Mode I and Mode II operation) is applied to the inverter at the V_{DC} value. The control pulse is deleted in the fourth cycle and the zero voltage (in the Mode III operation) is applied to the inverter. The transmission pulse is deleted in the fourth cycle and the zero voltage (in the Mode III operation) is applied to the inverter. When the four resonant cycles are considered, the output voltage of the inverter is seen to be in periodic waveform. The average output power is 3/4 when compared to full power operation. That is, the output power of the inverter is controlled by adjusting the square wave voltage (Vab).

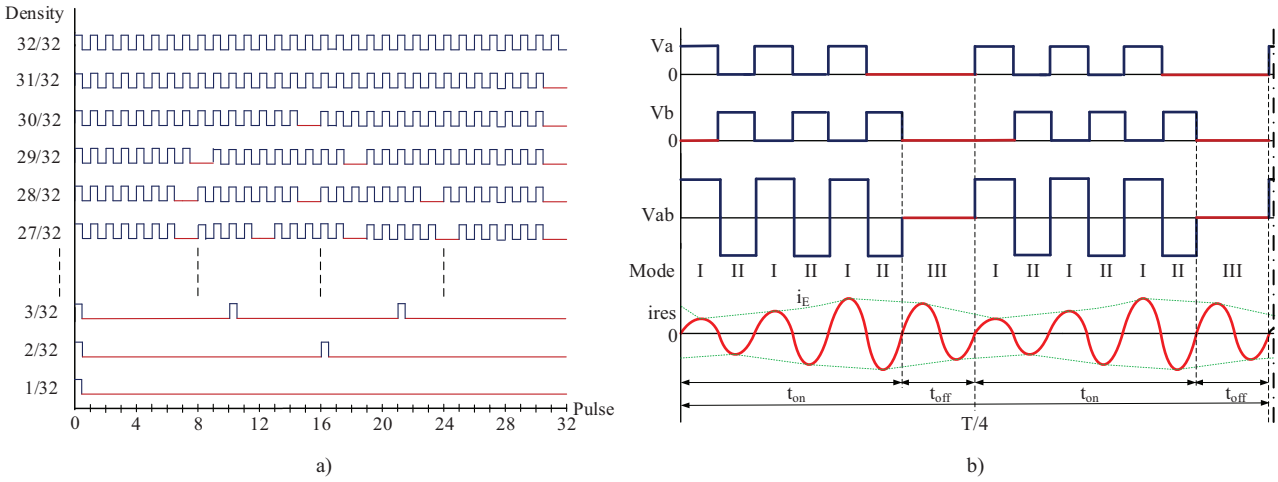

Figure 3. (a) The proposed 32 PDM patterns, (b) PDM current wave form.

The turn-on and turn-off durations of the switches are calculated by Equation 7;

$$T = NT_r = T_{on} + T_{off},\ T_{on} = N_1T_r,\ T_{off} = N_2T_r,\ D = \frac{T_{on}}{T} \tag{7}$$

In this equation, N is the resonant cycle number, N_1 is the normal resonant cycle number, and N_2 is the controlled (deleted pulses) resonant cycle number [23]. When the PDM control technique is applied to the series resonant circuit with a quality factor greater than 1 ($Q >> 1$), the resonant current has a sinusoidal form. Figure 4 shows the resonant current ($ires$) and the i_E is the current on the outside. In this case, the resonant current and the i_E current expressions are calculated by Equations 8 and 9.

$$i_E(t) = I(1 - e^{-at}) + I_{min}e^{-at},\quad 0 < t < t_{on} \tag{8}$$

$$i_E(t) = i_E(t_{on})e^{-a(t-t_{on})},\quad t_{on} < t < T \tag{9}$$

In this equation, I current is the maximum current $t_{on}/T = 1$, this is the Mode I and Mode II operation

condition. I_{min} value is obtained in the case of $t = 0$. The average output power is calculated by Equation 10;

$$P = \frac{4V_{DC}}{T\pi} \int_0^{t_{on}} i_E (sin\omega_r t)^2 dt \tag{10}$$

Accordingly, by using Equations 8 and 9, the average output power and the maximum power are found by Equations 11 and 12.

$$P = P_{max}[\frac{t_{on}}{T} + \frac{\tau}{T}(\frac{1 - e^{-at_{on}}}{1 - e^{-aT}})(e^{-at_{on}} - e^{-aT})] \tag{11}$$

$$P_{max} = \frac{2}{\pi} V_{DC} I cos\varnothing \tag{12}$$

Maximum power absorbed by the load for $t_{on}/T = 1$. τ is the time constant and $\varnothing$ is the phase angle. The phase angle is the angle between the resonant current and the fundamental square wave voltage. The time constant and the phase angle are calculated by the following equations, respectively.

$$\tau = \frac{2L}{R} \tag{13}$$

$$\varnothing = arctan[Q(\frac{\omega_s}{\omega_r} - \frac{\omega_r}{\omega_s})] \tag{14}$$

The phase angle at the resonant frequency is 0^o. If the PDM period ($T = NT_r$) is smaller than the time constant, the amplitude of the resonant current ($T << \tau$) is proportional to the pulse density. In this case, Equation 15 is obtained when the relationship between the output power and the pulse density is written.

$$\lim_{\tau \to \infty} P = P_{max} D^2 \tag{15}$$

If the PDM period ($T = NT_r$) is bigger than the time constant ($T >> \tau$), the output power is calculated by Equation 16 [25].

$$\lim_{\tau \to 0} P = P_{max} D \tag{16}$$

2.3. Sliding mode controlled PLL

The control system that locks the phase of the input signal and the output signal is called PLL control [9]. With the PLL, zero transitions of the current signal on the resonant circuit are detected, and the system is locked at the resonant frequency. Thus, the resonant frequency can be tracked quickly. In this way, zero switching points are detected, and the soft switching conditions are provided at the resonant frequency. The block diagram of the conventional PLL control circuit is shown in Figure 4.

Although the conventional PLL can achieve its stated goal, it has many shortcomings that reduce its performance. The natural phase locking operation of the conventional PLL can be very slow and unreliable. Conventional PLL is very sensitive to external disturbing factors such as mechanical vibrations. In addition, VCO parametric uncertainties cause a decrease in performance. SMC can be used for eliminating these shortcomings as it has a very robust structure against system uncertainties and external disturbances. Therefore,

it makes faster and more stable phase locking than the conventional PLL. It does not need an external phase locking detector. The block diagram of the sliding-mode-controlled PLL used in the proposed IH system is given in Figure 5. In addition, the flow chart of the sliding-mode-controlled PLL is given in Figure 6.

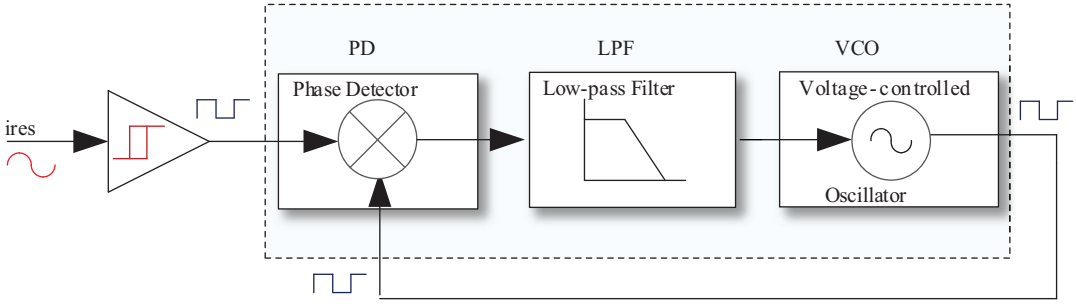

Figure 4. The block diagram of the conventional PLL function.

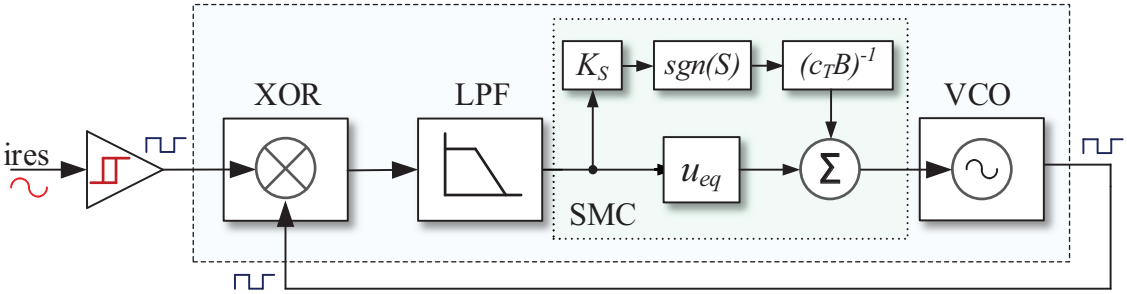

Figure 5. The block diagram of sliding-mode-controlled PLL function.

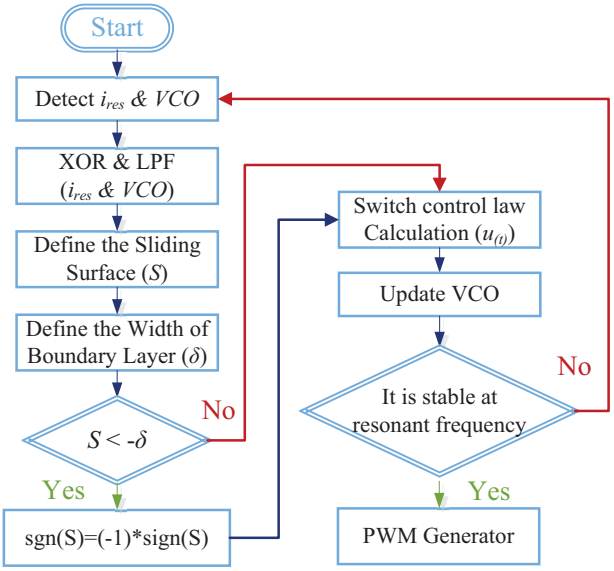

Figure 6. The flow chart of sliding-mode-controlled PLL function.

The power switches in the inverter must be operated at the resonant frequency to be switched on and off under ZCS conditions. For this purpose, it is necessary to determine whether the resonant circuit operates at the resonant frequency, or whether it is leading or lagging. In order to determine this, the graph given in Figure 7 is used according to the output of the low-pass filter (LPF).

As can be seen from the LPF output, the filter output is 0 only at the resonant frequency, while the filter output for other frequencies is at different voltages. Therefore, while the zero phase can be distinguished from the output of the filter, the other two phases are indistinguishable. Therefore, it is necessary to determine which phase the resonant circuit is operating at before the switching frequency fs is updated. For this, the operating phase of the resonant circuit is determined using the SMC algorithm. Using Figure 7, if the fs and V_{LPF} intersection is at point X_1 and a deviation is applied in the negative direction to the switching frequency, the new intersection point will be X_2.

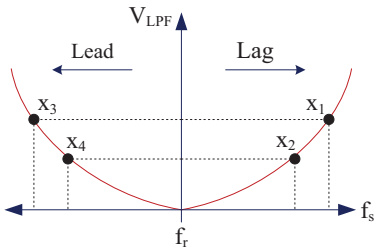

Figure 7. Three different phases varying according to the switching frequency.

If the same condition is applied to the points of X_3 and X_4, the result will be the opposite of the previous one. In order for the system to operate in continuous resonant, the LPF output must be kept at 0 continuously. Thus, the microcontroller with the proposed SMC-PLL generates the switching frequency according to the LPF output errors. The purpose of applying the SMC method to the closed-loop control systems is to send the error to the sliding surface, or alternatively, to the switching surface and to keep the error on this surface. For a good transient response and a minimum steady-state error, the switching surfaces can be integral and can be defined as follows [26]:

$$S_F = e_F(t) + K_F \int_0^t e_F(\tau)d\tau - e_F(0) \tag{17}$$

In this equation, $e_F = V_{ref}V_{LPF}$ is the error between the reference value (0) and the transient real values of the LPF output. K_F is the positive control gain. $S_F = 0$ manifold status indicates that the resonant frequency is fully tracked. Consequently, the following equations can provide a sufficient condition for the occurrence of the sliding mode:

$$\frac{de_F(t)}{dt} = -K_F e_F(t) \tag{18}$$

The purpose of designing the SMC law in the proposed system is to force the system trajectory for switching surface interaction to operate the inverter at the resonant frequency. This can be obtained by deriving Equation 19.

$$\frac{dS_F(t)}{dt} = \frac{de_F(t)}{dt} + K_F e_F(t) = -\frac{d}{dt}V_{LPF} + K_F(V_{ref}V_{LPF}) \tag{19}$$

After calculating the sliding surface, the state space equation of the VCO gain required for the calculation of the sliding mode control (u) is written as follows:

$$\dot{\mathbf{x}} = \mathbf{A}x + \mathbf{B}u + \mathbf{D} \tag{20}$$

The expressions are defined as; x ϵR^n, A ϵF^n, u ϵR^n, B ϵF^n, D ϵF^n . A and B represent the state space matrix, D represents the disorder and uncertainty. A and B matrices can be controllable, and D is assumed to be traceable. The formula of the sliding surface is written again.

$$S_F = c^T[\mathbf{A}x + \mathbf{B}u + \mathbf{D}] \tag{21}$$

In this equation, $c^T \epsilon R^n$ is the sliding surface coefficient. If the coefficient D is determined correctly by modeling, the system is perfectly controlled. However, since D is usually an unknown coefficient, Equation 22 is used to control the system more precisely.

$$\frac{dS_F(t)}{dt} = c^T[\hat{\mathbf{A}}x + \hat{\mathbf{B}}u] \tag{22}$$

Quadratic Lyapunov function and the time deviation of the function is as follows [26]:

$$W = \frac{1}{2}S^T S \tag{23}$$

$$\frac{dW}{dt} = S^T\frac{dS}{dt} = S^T(c^T[\hat{\mathbf{A}}x + \hat{\mathbf{B}}u]) \tag{24}$$

When $S \neq 0$, the control law W derivative should be determined correctly to be negative. Accordingly, the equivalent control given is as follows:

$$u_{eq} = -(c^T\hat{\mathbf{B}})^{-1}c^T[\hat{\mathbf{A}} + I]x \tag{25}$$

The control law of the sliding surface is given as follows:

$$u(t) = u_{eq} - (c^T\hat{\mathbf{B}})^{-1}K_S sgn(S) \tag{26}$$

In this equation, sgn(S) is the discontinuous controller. K_S is a scaling coefficient. This coefficient ensures the robustness of the SMC. The resonant frequency of the inverter is rapidly tracked by the SMC method. However, rapid transitions can cause unexpected chattering. This is undesirable because it can lead to unpredictable instability. To overcome this drawback, the discontinuous part of the controller is softened using a boundary layer around the sliding surface. As a result, the continuous function around the sliding surface is as follows:

$$sgn(S) = \begin{cases} 1, & if \quad S>\delta \\ \frac{S}{\delta}, & if \quad |S|\leq\delta \\ -1, & if \quad S<-\delta \end{cases} \tag{27}$$

In this equation, $\delta > 0$ represents the width of the boundary layer. The principle of the sliding mode control and the boundary layer are given in Figure 8. Thus, using Equations 25 and 26, the switching frequency reference of the inverter is obtained, and the resonant frequency is transmitted to the gate drive in the inverter to drive the switches.

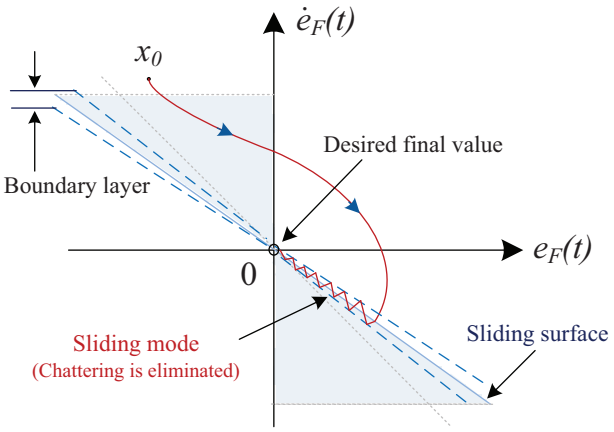

Figure 8. The principle of the sliding mode control and the boundary layer.

3. Simulation results

PSIM simulation circuit of the proposed SMC-controlled IH system is given in Figure 9. In order to evaluate the performance of the SMC-PLL algorithm, the traditional PI-controlled PLL algorithm was also developed, and the two algorithms were compared. For PI control, an error was found by finding the difference between the VCO output and PD. The resonant frequency was achieved by reducing this error to zero by using the PI controller. The equation used for this process is as follows.

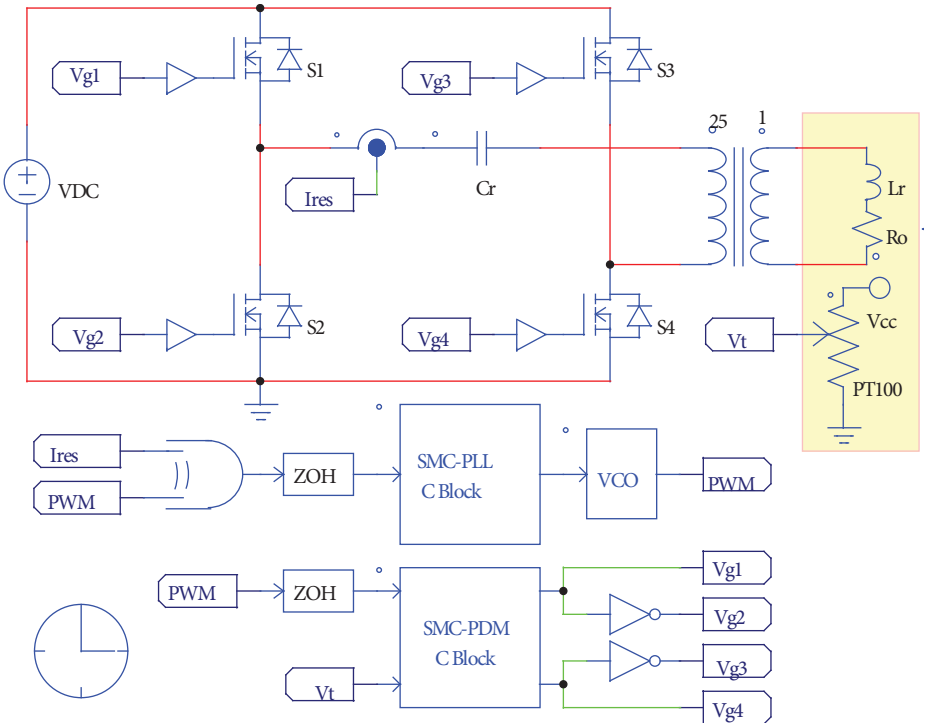

Figure 9. PSIM circuit of the proposed IH system.

$$PI = K_P e_{VCO}(t) + K_i \int_0^t e_{VCO}(t)dt \tag{28}$$

In this equation, e_{VCO} = VCO – PD, K_P is the positive proportional control gain, and K_i is the positive integral control gain. The PT100 sensor used for temperature feedback in the simulation study is modeled as an adjustable resistor. The SMC-PLL and PI-PLL algorithms were written in C language using the C block in the PSIM. The sampling frequency was determined as 200 kHz for the system to be dynamic. The parameters of the simulation model and the applied system are given in Table 1. The control parameters of the simulation and the experimental model are given in Table 2.

Table 1. Specifications of IH system.

Components	Symbol	Values
Output power	P_o	250 W
Input voltage	V_{DC}	50 V
Switching frequency	fs	33-42 kHz
Resonant inductance	L	400 μH
Resonant capacitor	C	44.8 nF
Resistance	R	12 Ω
Transformer ratio	$n_1 : n_2$	25:1
PDM pattern	N	32

Table 2. Control parameters.

Parameters	Values
Positive gains K_F	9000
Control gains K_S	10^6
Width of boundary layer δ	100
Positive proportional gains K_P	15
Positive integral gains K_i	2.3

In the simulation study, it was assumed that the active/passive circuit elements on the primary and secondary sides were ideal and there were no transmission losses. As seen from the simulation circuit, the single input of the SMC-PLL algorithm is the output of the XOR port. The resonant current converted to the square wave with a comparator and the PWM signal generated constitute the input of the XOR gate. When the system was first started, it was started above the resonant frequency so that the switches were not damaged.

As shown in Figure 10, both the SMC-PLL and the PI-PLL algorithms were tested by running the system with the initial switching frequency of 42 kHz. When the simulation results are examined, it is seen that the SMC-PLL algorithm tracks the resonance frequency more dynamically than the PI-PLL algorithm and eliminated the phase difference between the voltage and the current.

According to the simulation results, the SMC-PLL algorithm enables the system to operate at the initial switching frequency of 42 kHz and to settle at the resonant frequency of 37.5 kHz in 0.6 ms. PI-PLL algorithm reaches the resonant frequency in about 1.6 ms. Therefore, the proposed SMC-PLL algorithm is found to be

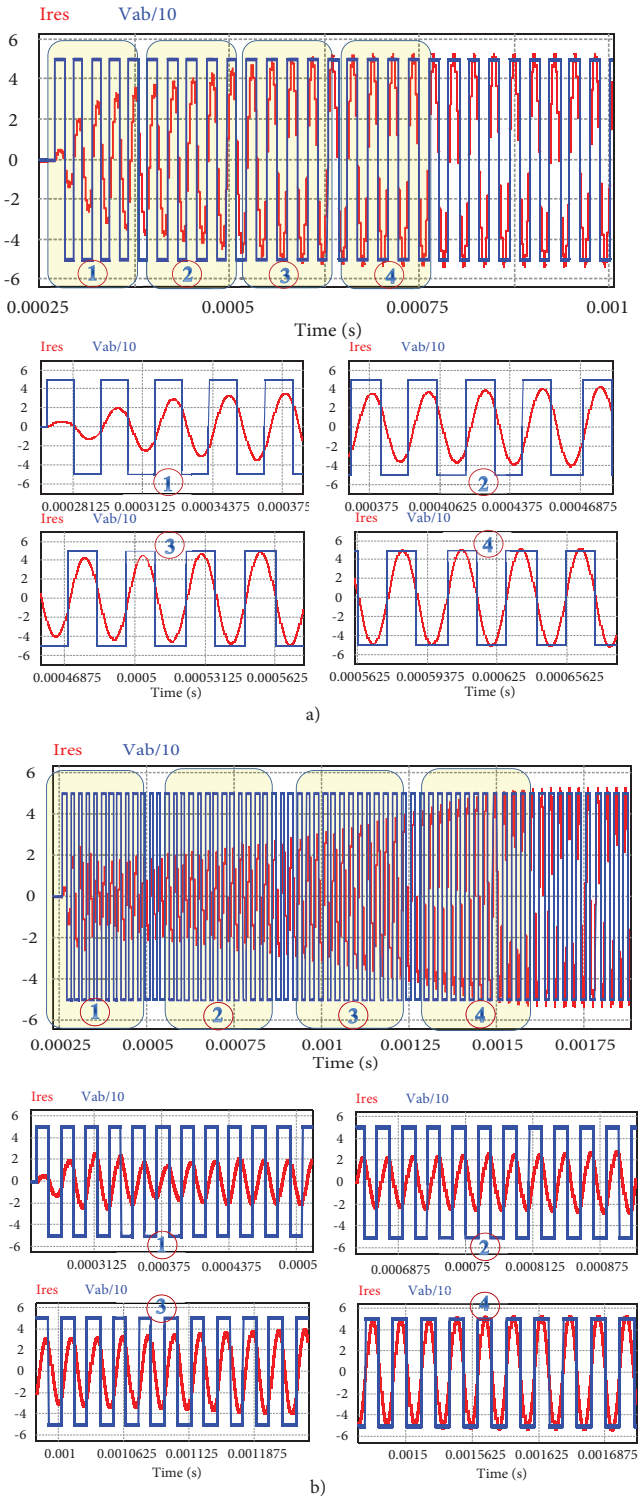

Figure 10. Start-up simulation results of the PLL algorithms for 42 kHz initial switching frequency, a) proposed SMC-PLL, b) PI-PLL.

quite fast, dynamic, and stable. The simulation responses of the PLL error for the proposed SMC-PLL and PI-PLL are given in Figure 11. On the other hand, as it is seen in Figure 12, although some of the switching signals are deleted in different PDM values (N=32, N=28, N=26, N=21), SMC-PLL algorithm operates in a continuous resonant by controlling the system very robustly.

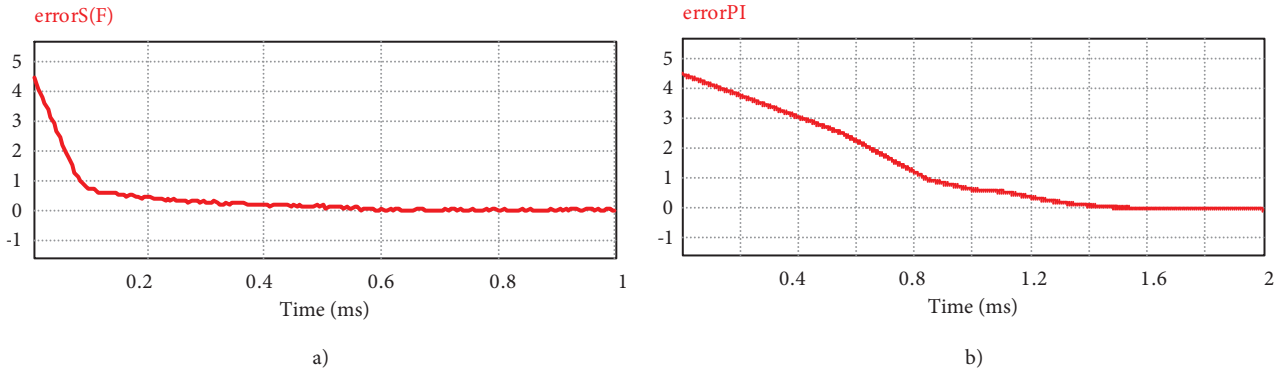

Figure 11. Simulation responses of the PLL error for (a) the proposed SMC-PLL and (b) PI-PLL.

4. Experimental results

For the proposed SMC-controlled IH system, an experimental setup was established in the laboratory. In the IH system, a 200 V 50 A IRFP260N was used as the power switch in the inverter circuit. The TLP250 optodriver with an output current of 1.5 A was used to drive the power switches. To detect the resonant current, a current transformer coiled up by 1:50 ratio on the toroid was used. The LM393 comparator integral was used to convert the sinusoidal resonant current to the square wave. CD4030M was used as the XOR gate to detect the resonant frequency. The high-frequency transformer was used in the 25:1 winding between the inverter and the induction coil. The stainless steel work piece used in the experimental setup was 200 mm long, 32 mm in diameter, and 1 mm in wall thickness. The PT100 K-Thermocouple and MAX6675 with 12-bit ADC were used for the temperature measurement of the work piece. As the heater insert, a copper pipe with a diameter of 6 mm was coiled up with eight windings, and a diameter induction coil with 60 mm diameter was designed. The ATMEL328P-AU microcontroller was used to control the SMC-PLL and PDM in the IH system. In the experimental study, Tektronix AA probe was used to measure the high-frequency resonant current. In addition, the Pintek voltage probe was used to measure the Vab voltage. Rigol oscilloscope was used to measure the circuit signals. Figure 13 shows the experimental setup.

Figure 14 shows the inverter output voltage (Vab) and inverter current (ires) at different PDM values for the steel work piece temperature to reach the desired temperature. Thus, the output power is controlled in the range of about 100 to 250 W. These waveforms are similar to the simulation results in Figure 12 and show that the designed system operates correctly.

As can be seen from the figures, since the inverter operates at the full resonant frequency in all PDM values, there is no phase difference between the resonant voltage and the current. Therefore, the resonant current is pure sinus and does not contain any harmonic component. The PDM-Temperature-Time graph shown in Figure 15 is obtained by transferring the data obtained by microcontroller from PT100 to the computer via the SCI protocol. As can be seen from the graph, the steel work piece with an initial temperature of 25 °C was heated, and it reached the set value in a short time.

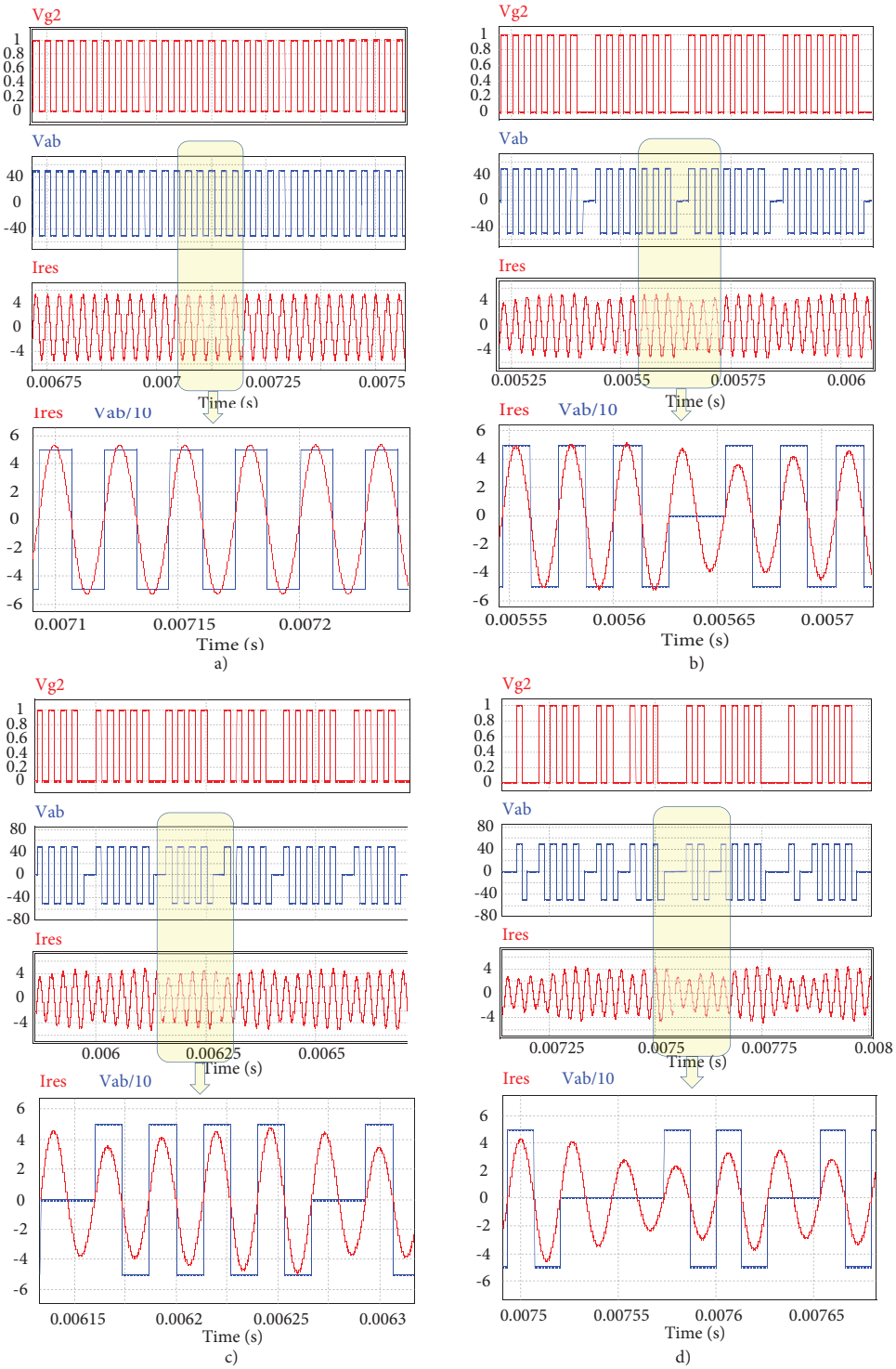

Figure 12. Simulation results of different PDM patterns: a) N = 32, b) N = 28, c) N = 26, d) N = 21.

The system was initially powered by N = 32 with the highest PDM value to achieve the desired temperature value of the steel work piece as quickly as possible. Then, when the temperature approached

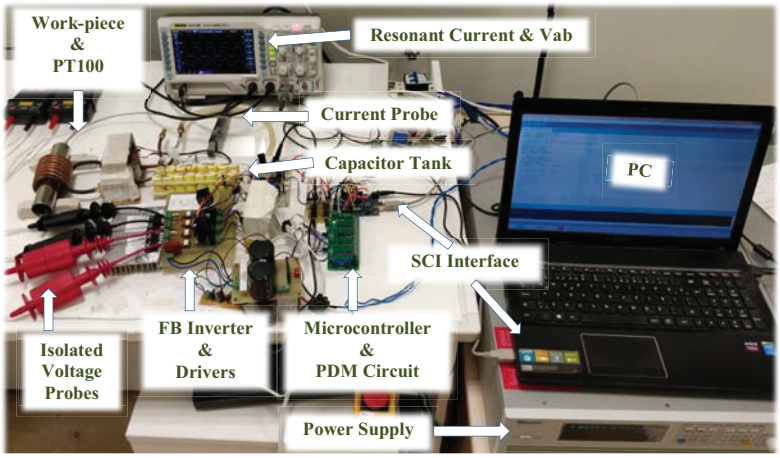

Figure 13. Experimental setup of the proposed IH system.

the set point, the PDM value began to decrease. The temperature of the work piece was set to 200 °C as shown in Figure 15. Accordingly, the PDM values range from N = 25 to N = 27 so that the temperature remains constant at this point. Thus, the inverter was operated in a stable manner at different PDM values, and the resonant frequency was continuously tracked by the SMC-PLL algorithm for these cases.

5. Conclusions

The aim of this study was to design a SMC-PLL algorithm for IH systems and to develop 32 PDM-controlled full bridge series resonant inverter. The designed SMC-PLL–controlled system was developed to have 250 W output power and to track the frequencies between 33 kHz and 42 kHz. The proposed system was validated by presenting the experimental results, calculations, and simulations. In the system, the power required for the work piece to reach the desired temperature in the IH system was controlled by deleting some of the control pulses of the series resonant inverter operated at the resonant frequency. Therefore, the output power was controlled in a wide range depending on the PDM value, and the ZCS was achieved continuously by tracking the resonant frequency quickly and correctly by the developed SMC-PLL algorithm. Thus, ZCS was provided continuously. Consequently, the current of the resonant circuit was pure sine and did not contain any harmonic component. In this way, the energy transfer from the primary side to the secondary side was carried out with minor losses. In addition, since the power switches of the inverter operated under ZCS conditions, on and off switching losses were also avoided. Since the SMC-PLL application was performed entirely digitally, an analog integrated circuit was not required. Therefore, the developed SMC-PLL application was found to be a cost-effective solution in addition to its flexible structure. In future studies, 16 or 8 PDM control algorithms can also be used. However, in this situation, the control precision of the output power can decrease, which will affect the precision in temperature control. As a result, it can be argued that 32 PDM control algorithm is more suitable in terms of power control. On the other hand, in the system, the PI and SMC control algorithms were compared and the proposed SMC-PLL performed better than PI-PLL. Different control algorithms except these algorithms can be used in the following studies.

Figure 14. Experimental waveforms of Vgate (CH1), Vab(CH2), and ires (CH3) for a) N = 32, b) N = 28, c) N = 26, d) N = 21.

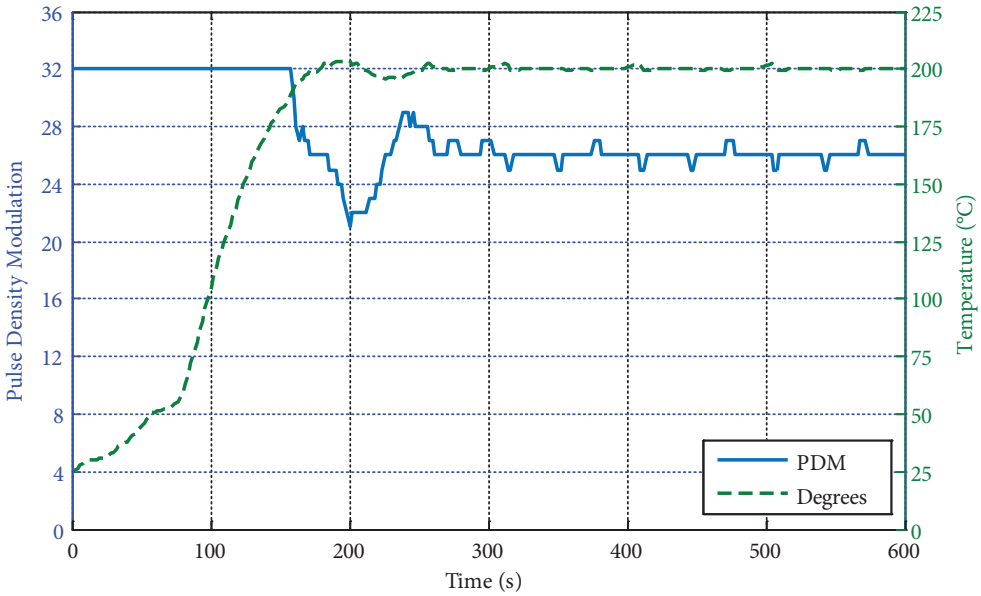

Figure 15. The PDM-temperature-time variation of the work piece.

Acknowledgments

This research was supported by Karabük University Research Fund (No: 14/2-DR-017) and Bandırma Onyedi Eylül University Research Fund (BANU BAP-19-1003-004). In addition, the author would like to thank Kenan Ünal for his support in the setup of the experimental hardware.

References

[1] Espi-Huerta JM, Santamaria EJDG, Gil RG. Castello-Moreno, J. Design of the L-LC resonant inverter for induction heating based on its equivalent SRI. IEEE Transactions on Industrial Electronics 2007; 54 (6): 3178-3187. doi: 10.1109/TIE.2007.905928

[2] Özbay H. PDM-MPPT based solar powered induction heating system. Engineering Science and Technology, an International Journal 2020. doi: 10.1016/j.jestch.2020.06.005

[3] Lucía O, Maussion P, Dede EJ, Burdío JM. Induction heating technology and its applications: past developments, current technology, and future challenges. IEEE Transactions on Industrial Electronics 2013; 61 (5): 2509-2520. doi: 10.1109/TIE.2013.2281162

[4] Rudnev V, Loveless D, Cook RL. Handbook of Induction Heating. Boca Raton, USA: CRC press, 2017.

[5] Llorente S, Monterde F, Burdio JM, Acero J. A comparative study of resonant inverter topologies used in induction cookers. In: 17th Annual IEEE Int. Conf. Applied Power Electronics, Dallas, USA; 2002. pp. 1168-1174.

[6] Suryawanshi HM, Pachpor S, Ajmal T, Talapur GG, Sathyan S et al. Hybrid control of high-efficient resonant converter for renewable energy system. IEEE Transactions on Industrial Informatics 2017; 14 (5): 1835-1845. doi: 10.1109/TII.2017.2756703

[7] Shu L, Chen W, Ma D, Ning G. Analysis of strategy for achieving zero-current switching in full-bridge converters. IEEE Transactions on Industrial Electronics 2017; 65 (7): 5509-5517. doi: 10.1109/TIE.2017.2779443

[8] Esteve V, Jordán J, Sanchis-Kilders E, Dede EJ, Maset E et al. Enhanced pulse-density-modulated power control for high-frequency induction heating inverters. IEEE Transactions on Industrial Electronics 2015; 62 (11): 6905-6914. doi : 10.1109/TIE.2015.2436352

[9] Chen MP, Chen JK, Murata K, Nakahara M, Harada K. Surge analysis of induction heating power supply with PLL. IEEE Transactions on Power Electronics 2001; 16 (5): 702-709. doi: 10.1109/63.949503

[10] Bal G, Oncu S, Ozbas E. Self-oscillated induction heater for absorption cooler. Elektronika ir Elektrotechnika 2013; 19 (10): 45-48. doi: 10.5755/j01.eee.19.10.5894

[11] Geng H, Sun J, Xiao S, Yang G. Modeling and implementation of an all digital phase-locked-loop for grid-voltage phase detection. IEEE Transactions on Industrial Informatics 2012; 9 (2): 772-780. doi: 10.1109/TII.2012.2209666

[12] Lin JM, Yang CY. A fast-locking all-digital phase-locked loop with dynamic loop bandwidth adjustment. IEEE Transactions on Circuits and Systems I: Regular Papers 2015; 62 (10): 2411-2422.

[13] Han B, Bae B. Novel phase-locked loop using adaptive linear combiner. IEEE Transactions on Power Delivery 2005; 21 (1): 513-514. doi: 10.1109/TPWRD.2005.860436

[14] Namadmalan A. Universal tuning system for series-resonant induction heating applications. IEEE Transactions on Industrial Electronics 2016; 64 (4): 2801-2808. doi: 10.1109/TIE.2016.2638399

[15] Zeng SQ. The application design and study of phase-locked loop CD4046. Electronics Quality 2012; (1): 25-72.

[16] Zhang K, Pu j. Low power consumption phase-locked loop 4046 applied research and simulation. Poplar Science and Technology 2014; (6): 124-126.

[17] Li S, Deng X. The design of phase-locked-loop circuit for precision capacitance micrometer. In: MATEC Web of Conferences 2016; (68): 12006-12009.

[18] Perruquetti W, Barbot JP. Sliding Mode Control in Engineering. Boca Raton, USA: CRC press, 2002.

[19] Yaylacı E K, Yazıcı İ. Sensorless double integral sliding mode MPPT control for the WECS. Journal of Renewable and Sustainable Energy 2018; 10 (2): 023301. doi: 10.1063/1.5001549

[20] Komurcugil H, Bayhan S, Abu-Rub H. Lyapunov-function based control approach with cascaded PR controllers for single-phase grid-tied LCL-filtered quasi-Z-source inverters. In: 2017 11th IEEE International Conference on Compatibility, Power Electronics and Power Engineering 2017; 510-515.

[21] Park NJ, Lee DY, Hyun DS. A power-control scheme with constant switching frequency in class-D inverter for induction-heating jar application. IEEE Transactions on Industrial Electronics 2007; 54 (3): 1252-1260. doi: 10.1109/TIE.2007.892741

[22] Lo YK, Lin CY, Hsieh MT, Lin CY. Phase-shifted full-bridge series-resonant DC-DC converters for wide load variations. IEEE Transactions on Industrial Electronics 2010; 58 (6): 2572-2575. doi: 10.1109/TIE.2010.2058076

[23] Karafil A, Ozbay H, Oncu S. Power control of resonant converter MPPT by pulse density modulation. In: 10th IEEE International Conference on Electrical and Electronics Engineering, Bursa 2017; 360-364.

[24] Nagarajan B, Sathi RR. Phase locked loop based pulse density modulation scheme for the power control of induction heating applications. Journal of Power Electronics 2015; 15 (1): 65-77. doi: 10.6113/JPE.2015.15.1.65

[25] Karafil A, Ozbay H, Oncu S. Design and Analysis of Single Phase Grid Tied Inverter with PDM MPPT Controlled Converter. IEEE Transactions on Power Electronics 2020; 35 (5): 4756-4766. doi: 10.1109/TPEL.2019.2944617

[26] Özbay H, Öncü S, Kesler M. SMC-DPC based active and reactive power control of grid-tied three phase inverter for PV systems. International Journal of Hydrogen Energy 2017; 42 (28): 17713-17722. doi: 10.1016/j.ijhydene.2017.04.020